Science Advances
AAAS

advances.sciencemag.org/cgi/content/full/4/11/eaat9744/DC1

Supplementary Materials for

Ion-induced sulfuric acid–ammonia nucleation drives particle formation in coastal Antarctica

T. Jokinen*, M. Sipilä, J. Kontkanen, V. Vakkari, P. Tisler, E.-M. Duplissy, H. Junninen, J. Kangasluoma, H. E. Manninen, T. Petäjä, M. Kulmala, D. R. Worsnop, J. Kirkby, A. Virkkula, V.-M. Kerminen

*Corresponding author. Email: tuija.jokinen@helsinki.fi

Published 28 November 2018, *Sci. Adv.* **4**, eaat9744 (2018)
DOI: 10.1126/sciadv.aat9744

This PDF file includes:

Section S1. Field site and instrumentation
Section S2. Methods
Table S1. Data coverage of individual instruments during the FINNARP 2014 campaign.
Table S2. Sulfuric acid concentration, condensation sink, particle growth rates, and particle formation rates for 3-nm (J_3) and 1.5-nm ($J_{1.5}$) particles determined for NPF events using different methods.
Fig. S1. Overview of the FINNARP 2014 campaign at Aboa, Antarctica (no flagged data).
Fig. S2. NPF days.
Fig. S3. No NPF days.
Fig. S4. Negative ion composition measured by the APi-TOF.
Fig. S5. APi-TOF (positive ions) mass defect plot during the observed NPF event on 18 January at Aboa.
Fig. S6. NAIS size distribution of negative (top) and positive (bottom) ions during the NPF event day when chemical composition of ion was measured in the positive polarity (fig. S5).
Fig. S7. Number concentrations of 1.5- to 3-nm particles during 1 week of the measurement period (4 to 10 January 2015).
Fig. S8. The size distribution of 2- to 42-nm particles (top), 0.8- to 42-nm negative (second) and positive (third) ions measured with the NAIS, and the sum of particle concentration measured with the PSM [1.5 to 3 (±0.2) nm; bottom] during the measurement campaign.
References (*26*–*38*)

Section S1. Field site and instrumentation

1.1. Finnish Antarctic research station

The Finnish Antarctic research station (Aboa) is located at the Queen Maud land, Eastern Antarctica (73°03'S, 13°25'W), on Basen nunatak in the Vestfjella Mountains. Aboa station is located around 130 km from open ocean and approximately 500 m above sea level. Detailed information about Aboa, the Finnish Antarctic research program (FINNARP) and FINNARP-2014 expedition are available at (http://www.antarctica.fi/in-english, 9. Aug 2018).

All aerosol and precursor molecule measurements were conducted from the aerosol measurement laboratory located 200 m upwind from the main station. Pollution from the station (mostly from vehicles and generator exhaust) is minimal due to the dominant North-Eastern (~45º) wind direction. Sampling was done ~3 m from ground level using instrument specific stainless steel or copper sampling inlets (~0.6 – 1.0 m in length).

Measurements were conducted with different particle counters, mass spectrometers and air ion spectrometers. Approximate data coverage is depicted in Table 1 (does not include short brakes or power cuts) and the instruments are introduced in details in the next chapters.

Table S1. Data coverage of individual instruments during the FINNARP 2014 campaign. The whole campaign was measured under midnight sun conditions (no sunsets or sunrises).

Instrument:	**Data Coverage:**
APi-TOF (negative ions)	30 Nov 2014 – 28 Jan 2015
APi-TOF (positive ions)	17 – 19 Jan 2015
CI-APi-TOF (aerosol precursor gases)	7 Dec 2014 – 28 Jan 2015
DMPS (particle size distribution, 6-820 nm)	29 Nov 2014 – 23 Jan 2015
PSM (particle size distribution, scanning, 1-3 nm)	30 Nov 2014 – 19 Jan 2015
NAIS (ion size distribution, 0.8-42 nm)	30 Nov 2014 – 28 Jan 2015
NAIS (particle size distribution, 2.25-42 nm)	30 Nov 2014 – 28 Jan 2015

1.2. APi-TOF

Atmospheric Pressure interface-Time of Flight (APi-TOF) (*26*) mass spectrometer was most of the time operated in the negative ion mode to detect ions and ion clusters during the campaign. We used 30 minutes averages when preprocessing the data to prevail changes in ion composition during the campaign. Inlet flow was kept at a constant ~10 Lpm (liters per minute) to minimize losses of low-volatile gases to the walls. Inlet line was a copper tube, 10 mm in diameter, ~1 m in length.

Positive polarity measurements were only conducted for two days in the end of the campaign (Table S1, Fig S5). All together eight NPF events were measured using negative and one using positive polarity ion composition measurements.

1.3. CI-APi-TOF

Chemical Ionization-Atmospheric Pressure interface-Time of Flight (CI-APi-TOF) (*27*) mass spectrometer was measuring sulfuric acid and other low-volatile compounds from 7 Dec 2014 until 28 Jan 2015. Chemical ionization mass spectrometers (CIMS) were originally developed for atmospheric sulfuric acid and MSA measurements. After replacing the original quadrupole mass spectrometer with a time-of-flight, the

instrument is now able to detect highly oxidized organic compounds, dimethylamine and iodine containing compounds among many other compounds (e.g. (*17*, *22*, *27*)).

The instrument was run in the negative ion mode with charged nitric acid (NO_3^-) as a reagent ion (3 sccm HNO_3- flow mixed with ~20 standard Lpm, sheath flow). Charging of nitric acid to nitrate ions was done by a soft X-ray source (L9490, Hamamatsu). The sample was pulled in via ~60 cm ¾" tube with a flow rate of around 10 Lpm. The sample was surrounded with sheath flow, which contained the reagent ions. The reagent ions were guided to mix with the sample using electric fields (ion source -125 V, drift tube -100 V). Sample was negatively charged either with proton transfer from the acidic sample molecule (AH) to the reagent ions (B) via $AH + B^- \rightarrow A^- + BH$ or clustering $AH + B- \rightarrow AHB^-$. More information of the CI-APi-TOF can be obtained from Jokinen et al. (2012) (*27*).

The concentration of low volatility molecules was calculated as following

$$[sample]_{neutral} = \frac{sample^- + sample \cdot NO_3^-}{\sum \text{reagent ions}} x\ C \quad (1)$$

where $[sample]_{neutral}$ is the calculated concentration (in molecules/cm^3) of the neutral measured compound e.g. SA and MSA, $sample^-$ is the measured signal of sample chemically charged sample charged via proton transfer, $sample \cdot NO_3^-$ is the measured charged sample signal formed via clustering. Reagent ions are the sum of observed nitrate signals: NO_3^-, $HNO_3NO_3^-$ and $(HNO_3)_2NO_3^-$and C is a calibration factor.

The instrument was calibrated using sulfuric acid and the concentrations are calculated using a calibration factor of $1.195 \cdot 10^{10}$ molecules/cm^3 obtained from this calibration. We also present error estimations rising from calibrations from previous studies done for this particular instrument. We present the data for low-volatile compound concentration as a low and high end estimation using low limit calibration factor of $C=5 \cdot 10^9$ (CI-inlet only, no losses to sampling line) and high limit factor $C=1.89 \cdot 10^{10}$ (including wall losses to the sampling line). CI-APi-TOF data showed in the article are 5-minute average values. Limit of detection (LOD) was determined using sulfuric acid and zero measurements, LOD = $3.6 \cdot 10^4$ molecules/cm^3.

1.4. Differential mobility particle sizer (DMPS)

Aerosol size distributions between 6 and 820 nm in diameter were measured using a differential mobility particle sizer (DMPS) technique (*28*). DMPS used in this study consisted of a C-14 radioactive aerosol neutralizer, medium length Vienna type (HAUKE) differential mobility analyzer and a TSI 3772 condensation particle counter.

1.5. Particle Size Magnifier (PSM)

The smallest nanoparticles were measured with a nano Condensation Nuclei Counter (nCNC, Airmodus). nCNC is a mixing-type condensation particle counter (CPC) and it is a combination of a Particle Size Magnifier (PSM) and a regular CPC (*29*). Please note that in this article, the whole nCNC-system is referred to as the PSM, as it is commonly done in the literature. Diethylene glycol is used to activate and grow particles to 90 nm inside the PSM. After this initial growth, particles are guided to the following CPC and treated with butanol vapour that grows these particles to sizes where they are detectable by the counter.

During the Aboa campaign, the cut-off size of one of the PSM was varied between approximately 1 and 3 nm (electrical mobility equivalent diameter) by altering the mixing ratio of the sample and saturator flow rates in two minute intervals. The conversion from the PSM saturator flow rate to the cut-off size contains uncertainties related to the particle chemical composition (*30 and references within*).

Presuming the cluster distributions in Aboa during particle formation event time are such that the number concentration increases toward smaller sizes in the PSM size range, the uncertainties in the measured particle concentrations are relatively large if no uncertainty in the cutoff is considered. Therefore we include uncertainties separately in the PSM cutoff diameter and measured size classified concentrations. Clusters observed in Aboa were expected to contain sulfuric acid and other inorganic compounds with very low concentration of organic compounds, and therefore the PSM was calibrated before the campaign using negatively charged ammonium-sulfate clusters generated with a tube furnace. The data inversion was conducted by assuming Gaussian-shaped kernel functions (*30*) so that the concentration of clusters in two size bins of 1.5–2 nm and 2–3 nm nm (± 0.2 nm) was obtained with time resolution of 12 min. In this case, when all clusters can be expected to be composed of sulfuric acid and ammonia, the uncertainty in the PSM

calibration due to particle composition can be expected to be relatively small. This statement contains the assumption that ammonium sulfate clusters activate with similar efficiency as sulfuric acid clusters. Therefore, the uncertainties in the inverted size bin limits reflect uncertainties in the particle activation due to the unknown particle charging state and varying sample flow rate water vapor composition. Kangasluoma et al. (2016) (*31*) have shown a difference of 0.2 nm in the PSM cutoff when measured for charged or neutral ammonium sulfate particles, translating to uncertainty of ± 0.1 nm. Changes in water vapor concentration have been also shown to affect the PSM lowest cutoff. However, changes in the water vapor concentration in our measurement site are much smaller than measured in laboratory experiments, therefore adding relatively small uncertainty to the PSM cutoffs (another ± 0.1 nm). These two sources of uncertainty combine into total of ± 0.2 nm uncertainty in the PSM cutoff limits. The uncertainties in the inverted concentrations originate from the inversion procedure (not constant particle concentration in the width of the PSM kernel, uncertainty in the PSM kernel, random noise) and measurement errors that are not easy to quantify. These uncertainties have been estimated using much higher particle concentrations (about a factor of 5 higher) and in here we thus give a rough estimate on the concentration uncertainty of the particle concentrations measured by the PSM, equal to concentration uncertainty of ± 50% for the PSM size classified concentrations with ± 0.2 nm size uncertainty.

1.6. Neutral cluster and Air Ion Spectrometer (NAIS)

Ion mobility spectrometer, Neutral cluster and Air Ion Spectrometer (NAIS), was measuring the size distributions of ions between 0.8 nm and 42 nm (mobility equivalent diameter) and total particles, i.e. neutral and charged, between ~2 nm and 42 nm in Aboa (*32*). When total particles are measured, the sample aerosol is charged with a corona charger. Two cylindrical differential mobility analyzers classify positive and negative ions based on their electrical mobility and 21 electrometers on the outer cylinder detect the ions. Diffusion losses were minimized using high sample flow rate (54 l/min). Time resolution of the NAIS data was 3 minutes. Ion concentration measurement uncertainty is ±30 %.

Section S2. Methods

2.1. Ion-ion recombination

To investigate the role of ion-mediated processes in particle formation in Aboa, we studied the contribution of ion-ion recombination to sub-3 nm particle concentrations. The concentration of recombination products was calculated for the size range of 1.5–3 (±0.2) nm from (*33*)

$$N_{rec} = \frac{\alpha \sum_{j,k} r_{jk} N_j^+ N_j^- -}{CoagS} \quad (2)$$

Here α is the ion–ion recombination coefficient for which the value of 1.6×10^{-6} cm^3 s^{-1} is commonly used. N_j^+ and N_k^- are the concentrations of positive and negative ions in the size bins *j* and *k*, respectively, and r_{jk} tells the fraction of the recombination products formed in their collisions that ends up in the studied size range. CoagS refers to the average coagulation sink of the size range. Thus, Eq. (2) takes into account the production of neutral particles in the collisions between two oppositely charged ions and their loss by coagulation. The effect of the growth of recombination products out of the studied size range was neglected. The ion concentrations needed for calculating the recombination production rate were obtained from ion size distribution data measured with the NAIS (see (*33*)). The coagulation sink was calculated from particle size distributions measured with the DMPS (*34*).

2.2. Particle growth rates

Distinct NPF events with an appearance of nucleation mode particles and their subsequent growth to larger sizes were observed on nine days (3, 7-11,13, 18 and 20 January 2015). Particle growth rates (GR) were determined for NPF events using several different methods.

From DMPS data, GRs were determined by using lognormal distribution function method (*34*). First, lognormal distribution functions were fitted to particle number size distributions at each time step. Then, GR was retrieved as the slope of a linear least-square fit to the geometric mean diameters of growing nucleation mode and the corresponding times. Using this method it was possible to determine GR for the 6–10 nm size range for three NPF events (7, 8 and 13 January 2015).

From NAIS particle mode data, GRs were determined using maximum-concentration method (*34*). First, the times at which particle concentration in each size bin reaches its maximum were determined by fitting a Gaussian distribution to the concentration time series. Then, the growth rate was obtained as the slope of a linear least-square fit to the moments of maximum concentrations and the geometric mean diameters of each size bin. Using this method, it was possible to determine GR for the 5–10 nm size range for one NPF event (7 January 2015).

GRs were also determined using measured sulfuric acid concentration. This was done by determining sulfuric acid concentration for each NPF event and then calculating GR explained by kinetic condensation of sulfuric acid on 3 nm particles according to Nieminen et al., 2010 (*35*). Using this method, we were able to calculate GRs for all the observed NPF events during the campaign.

The obtained GRs are shown in Table S2. Ylijuuti et al. (2011) (*36*) compared GRs of nucleation mode particles determined from particle size distribution data by using different instruments and methods and concluded that the average uncertainty in GRs due to used instrumentation is ~25% for the smallest particles, and the average uncertainty due to analysis method is on the same order. The uncertainty of GRs explained by sulfuric acid condensation caused by uncertainty in sulfuric acid measurement can be estimated to be about +100% -50%. When comparing GRs determined from measured particle size distributions and GRs explained by sulfuric acid condensation, it seems that sulfuric acid is, within the measurement uncertainties, able to explain the observed particle growth in Aboa.

2.3. Particle formation rates

The formation rate J of particles in the size range $[D_p, D_p + \Delta D_p]$ can be calculated from (*34*)

$$J_{Dp} = \frac{dN_{Dp}}{dt} + \frac{GR}{\Delta Dp} \cdot N_{Dp} + CoagS_{Dp} \cdot N_{Dp} \quad (3)$$

Here N_{Dp} is the concentration of particles in the size range, GR is the particle growth rate and $CoagS_{Dp}$ is the coagulation sink calculated from particle size distribution data. We applied Eq. (3) for calculating the formation rates of 3 nm particles (J_3) and 1.5 nm particles ($J_{1.5}$).

We calculated J_3 from Eq. (3) by using the particle concentration measured with the NAIS ($J_{3,NAIS}$) We used two different values for GRs: 1) GRs calculated from DMPS for 6–10 nm size range for three events (GR_{DMPS}) 2) GRs calculated based on sulfuric acid concentration (GR_{SA}). The values obtained for $J_{3,NAIS}$ are presented in Table 2. $J_{3,NAIS}$ obtained using the two different GRs were close to each other.

We calculated $J_{1.5}$ by using two different methods: 1) $J_{1.5,PSM}$ was calculated from Eq. (3) using particle concentration measured with the PSM and GRs calculated based on sulfuric acid concentration. 2) $J_{1.5,extrap}$ was calculated from J_3 values (calculated using SA_{GR}) applying the equation (*34*)

$$J_{1.5,extrap} = \frac{J_3}{exp\left(\gamma\left(\frac{1}{3}-\frac{1}{1.5}\right)\frac{CS'}{GR}\right)} \quad (4)$$

Here CS' is directly related to condensation sink CS (CS=4πD×CS', where D is the gas-phase diffusion coefficient of sulfuric acid). CS was calculated from the DMPS data. GR is the particle growth rate for which we used values calculated based on SA concentration. γ is a parameter for which the value of 0.23 nm^2 m^2 h^{-1} was used. The values obtained for $J_{1.5}$ using the two methods were on most of the days very similar (see Table S2).

Table S2. Sulfuric acid concentration, condensation sink, particle growth rates, and particle formation rates for 3-nm (J_3) and 1.5-nm ($J_{1.5}$) particles determined for NPF events using different methods.

Date in 2015	SA (cm^{-3})	CS (s^{-1})	GR_{DMPS} (nm/h)	GR_{NAIS} (nm/h)	GR_{SA} (nm/h)	$J_{3,NAIS}$ Using GR_{DMPS} (cm^{-3} s^{-1})	$J_{3,NAIS}$ using GR_{SA} (cm^{-3} s^{-1})	$J_{1.5,extrap}$ using GR_{SA} (cm^{-3} s^{-1})	$J1_5$ PSM using GR_{SA} (cm^{-3} s^{-1})
3. Jan	1.47E+07	3.2E-4	-	-	0.68	-	0.04	0.06	-
7. Jan	1.58E+07	1.6E-4	1.30	1.04	0.73	0.14	0.10	0.12	0.11
8. Jan	1.67E+07	1.4E-4	0.49	-	0.78	0.04	0.04	0.05	0.09
9. Jan	1.41E+07	3.3E-4	-	-	0.66	-	0.06	0.09	0.09
10. Jan	1.73E+07	2.9E-4	-	-	0.80	-	0.08	0.11	0.11
13. Jan	9.54E+06	3.5E-4	0.26	-	0.44	0.03	0.03	0.05	0.07
18. Jan	1.76E+07	3.3E-4	-	-	0.82	-	0.07	0.09	0.13

2.4. Parametrized nucleation rates

In Dunne et al., 2016 (*19*) a following parametrization is presented for ternary ion-induced nucleation rates

$$J = k(T)n\,\frac{[NH_3][H_2SO_4]^p}{a+\frac{[H_2SO_44]^p}{[NH_3]^pA}} \quad (5)$$

Here $k(T)$ is a temperature dependent rate coefficient, n is the concentration of small ions (one polarity) and $[NH_3]$ and $[H_2SO_4]$ are the concentrations of ammonia and sulfuric acid. p, p_A and a parameters for which the values of 3.14, 3.07 and 0.00485 were obtained by Dunne et al., 2016 (*19*).

We utilized this parametrization to calculate ternary ion-induced nucleation rates corresponding a range of sulfuric acid and ammonia concentrations. For temperature we used T = 268 K and small ion concentration were determined from NAIS ion mode data.

2.5. Ion production (GCR)

In steady state, when coagulation losses are neglected, negative ion concentrations can be estimated from

$$[N_{neg.\ ions}] = \frac{J_{neg,GCR}}{\alpha\,[N_{pos.ions}]} \quad (6)$$

Where $J_{neg,GCR}$ is the ion production rate due to galactic cosmic radiation, and α is the ion–ion recombination coefficient (1.6×10^{-6} cm^3 s^{-1}) (*33*).

If we assume N_{neg} and N_{pos} (concentration of negative and positive ions) as equal and $J_{neg,\,GCR}$ = 2 cm^{-3} s^{-1}, we can write the equation as following

$$[N_{neg.\ ions}] = \frac{J_{neg,GCR}}{\alpha\,[N_{neg}]} \rightarrow [N_{neg.ions}] = \sqrt{\frac{J_{neg,GCR}}{\alpha}} = 1118\ cm^{-3} \quad (7)$$

During the measurement at Aboa, we constantly measured lower ion concentrations than the theoretical maximum calculated in Eq. 7, indicating that galactic cosmic radiation is the sole source of ions at our measurement site, as can be expected due to the thick glacier preventing radon permeating the ice.

2.6. Air mass origin

Emission sensitivity of air masses during the 72 h before arrival at Aboa was calculated with Lagrangian particle dispersion model Flexpart version 9.02 (*37*). The European Centre for Medium-Range Weather Forecasts (ECMWF) operational forecast with 137 model levels, 1 h temporal resolution was used as input data to Flexpart. The ECMWF forecast was obtained at 0.15 degree latitude-longitude resolution for an area

of 85°S - 50°S and 90°W - 90°E. Only emission sensitivity within 600 m of the surface was taken into account to ensure that footprint over the ocean would be within the marine boundary layer. Daily sea ice coverage was obtained from NOAA/NSIDC Climate Data Record of Passive Microwave Sea Ice Concentration, Version 2 (*38*).

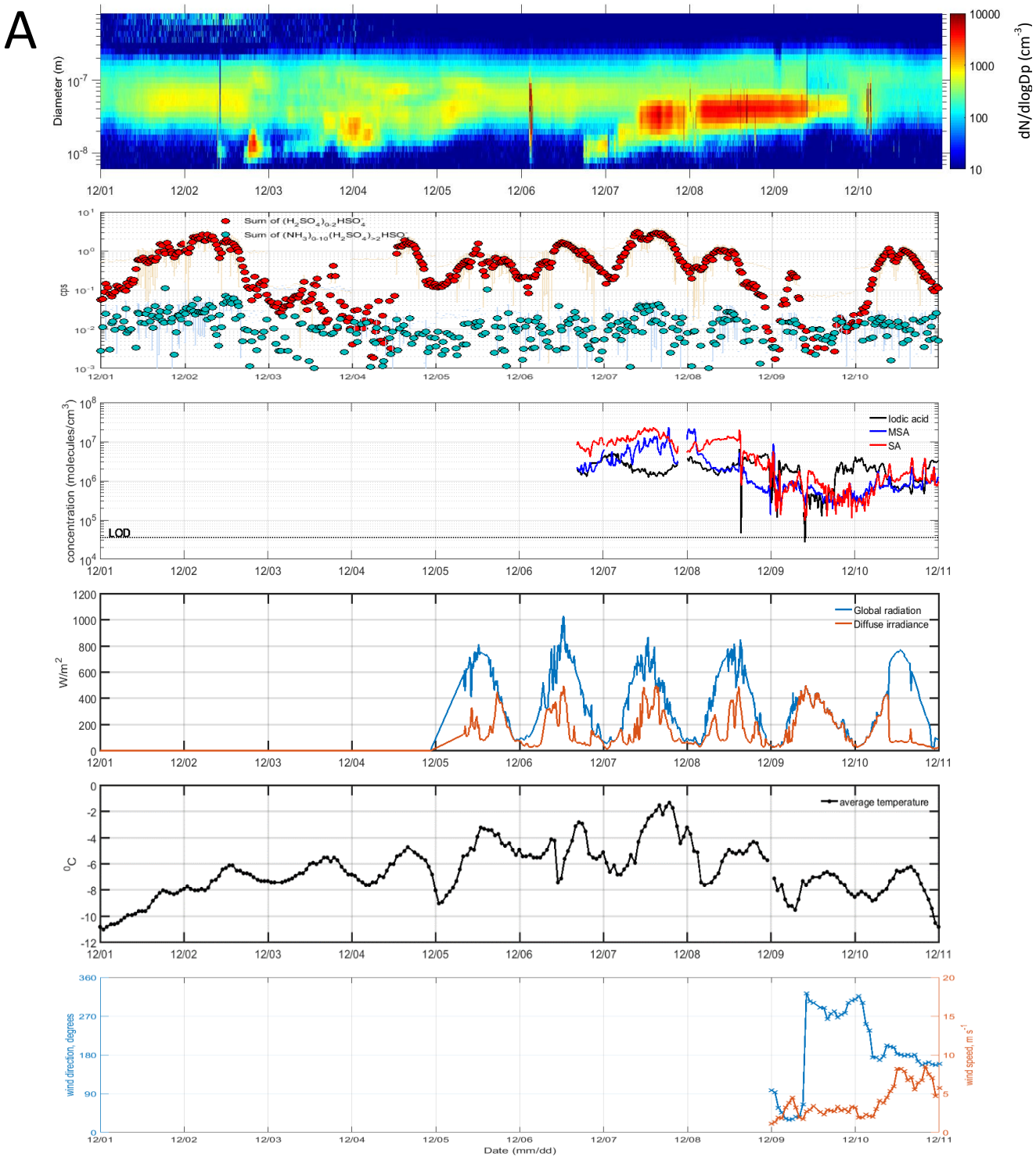
A
Diameter (m)
dN/dlogDp (cm-3)
10000
1000
100
10
Sum of (H2SO4)0-2HSO4
Sum of (NH3)0-10(H2SO4)>2HSO4
cps
concentration (molecules/cm3)
Iodic acid
MSA
SA
LOD
W/m2
Global radiation
Diffuse irradiance
average temperature
0C
wind direction, degrees
wind speed, m s-1
12/01
12/02
12/03
12/04
12/05
12/06
12/07
12/08
12/09
12/10
12/11
Date (mm/dd)

B

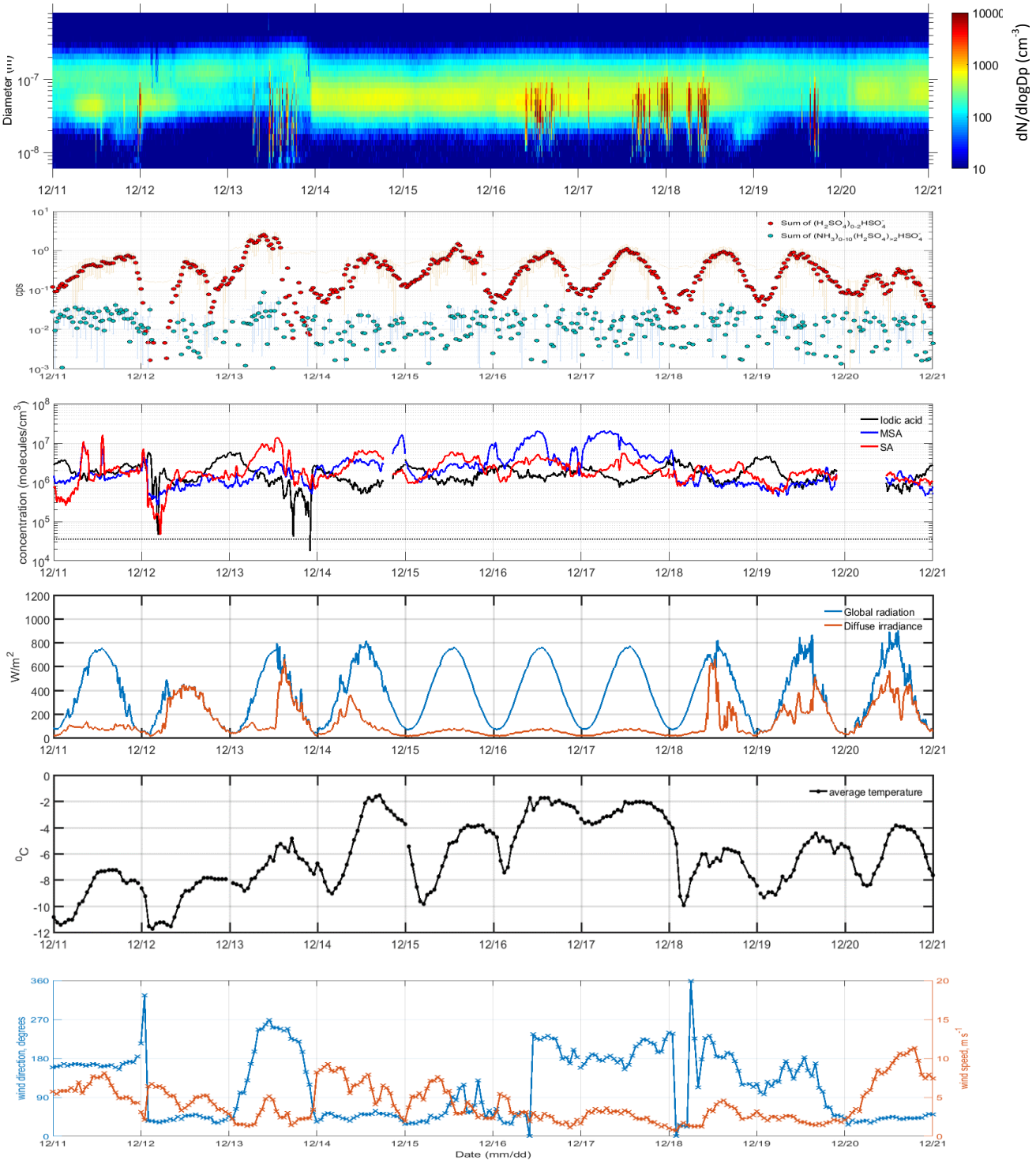
Diameter (m)
dN/dlogDp (cm-3)
cps
Sum of (H2SO4)0-2HSO4-
Sum of (NH3)0-10(H2SO4)>2HSO4-
concentration (molecules/cm3)
Iodic acid
MSA
SA
W/m2
Global radiation
Diffuse irradiance
0C
average temperature
wind direction, degrees
wind speed, m s-1
12/11
12/12
12/13
12/14
12/15
12/16
12/17
12/18
12/19
12/20
12/21
Date (mm/dd)

C

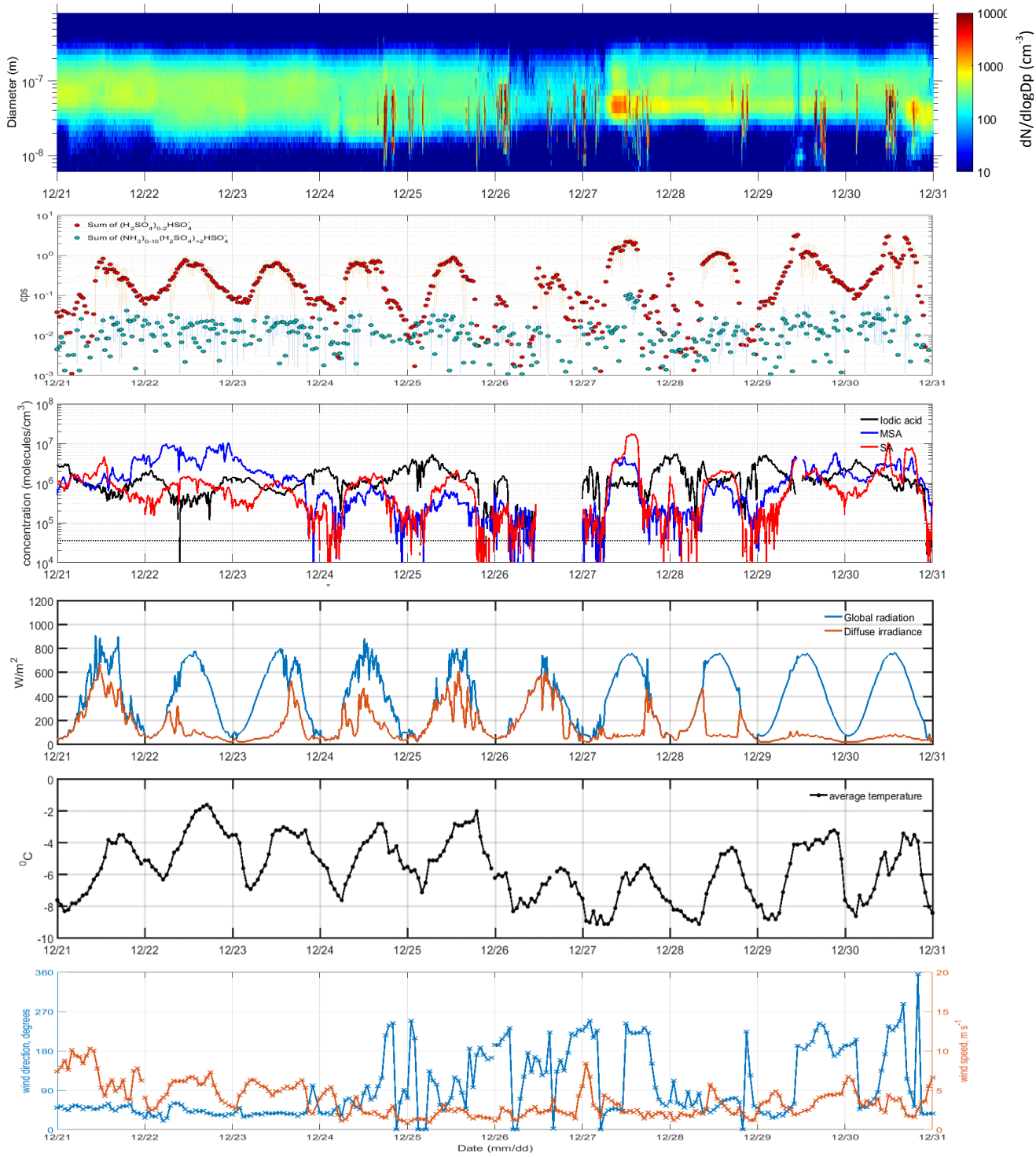
Diameter (m)
dN/dlogDp (cm-3)
cps
Sum of (H2SO4)0-2HSO4-
Sum of (NH3)0-10(H2SO4)1-2HSO4-
concentration (molecules/cm3)
Iodic acid
MSA
SA
W/m2
Global radiation
Diffuse irradiance
0C
average temperature
wind direction, degrees
wind speed, m s-1
12/21
12/22
12/23
12/24
12/25
12/26
12/27
12/28
12/29
12/30
12/31
Date (mm/dd)

D

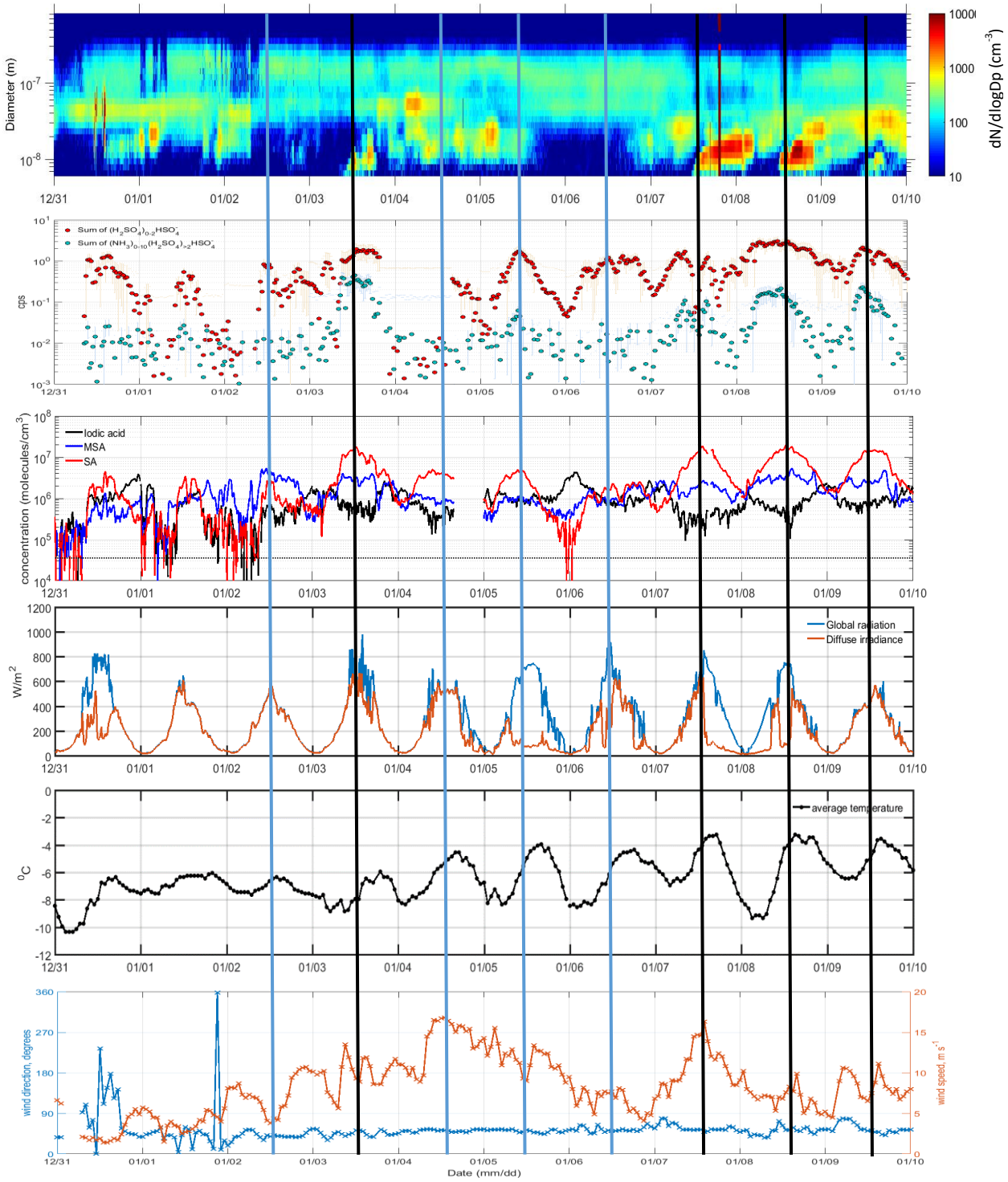
Diameter (m)
dN/dlogDp (cm-3)
cps
Sum of (H2SO4)0-2HSO4-
Sum of (NH3)0-10(H2SO4)>2HSO4-
concentration (molecules/cm3)
Iodic acid
MSA
SA
W/m2
Global radiation
Diffuse irradiance
0C
average temperature
wind direction, degrees
wind speed, m s-1
12/31
01/01
01/02
01/03
01/04
01/05
01/06
01/07
01/08
01/09
01/10
Date (mm/dd)

E

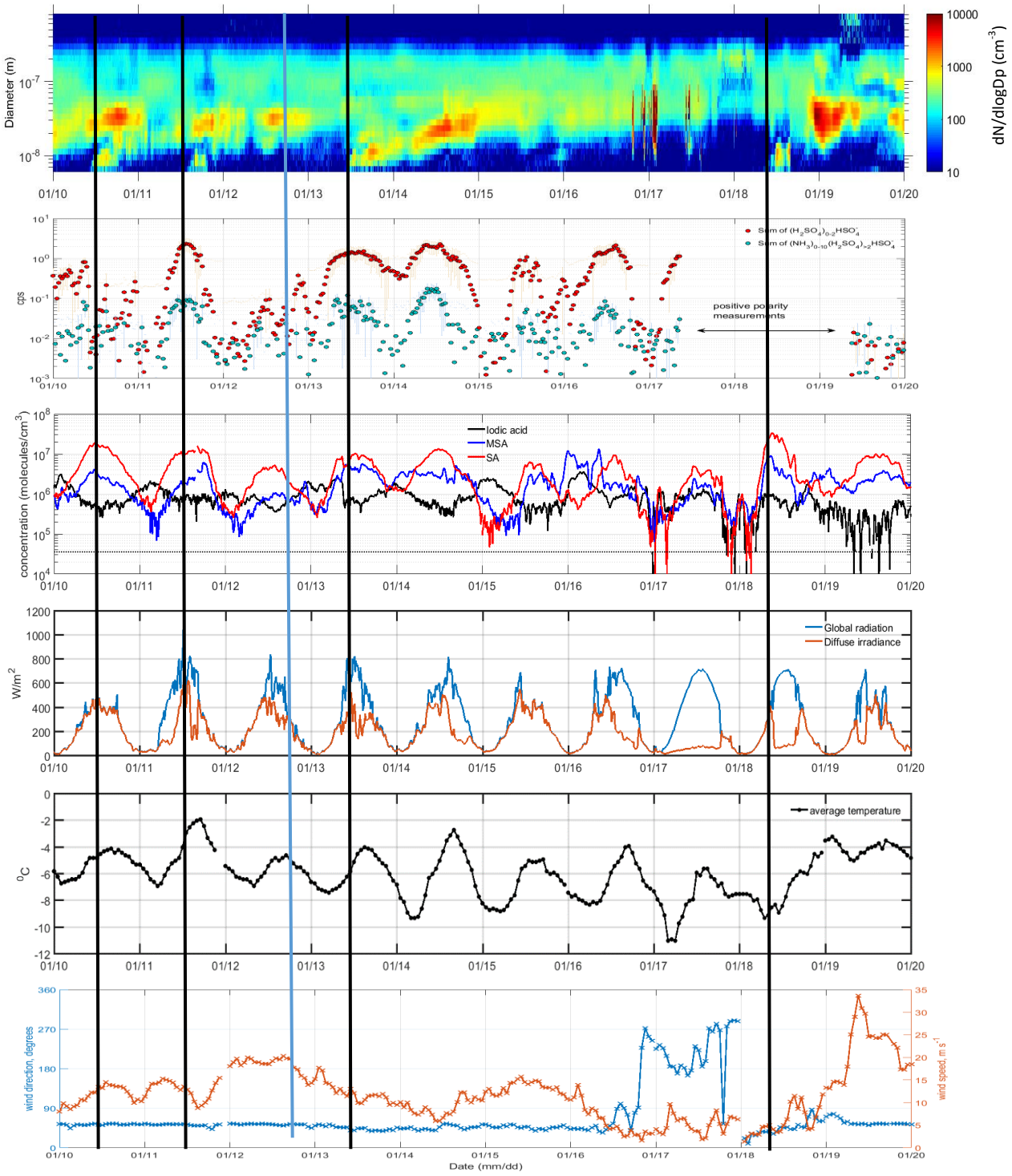
Diameter (m)
dN/dlogDp (cm-3)
cps
positive polarity measurements
concentration (molecules/cm3)
Iodic acid
MSA
SA
W/m2
Global radiation
Diffuse irradiance
°C
average temperature
wind direction, degrees
wind speed, m s-1
Date (mm/dd)

F

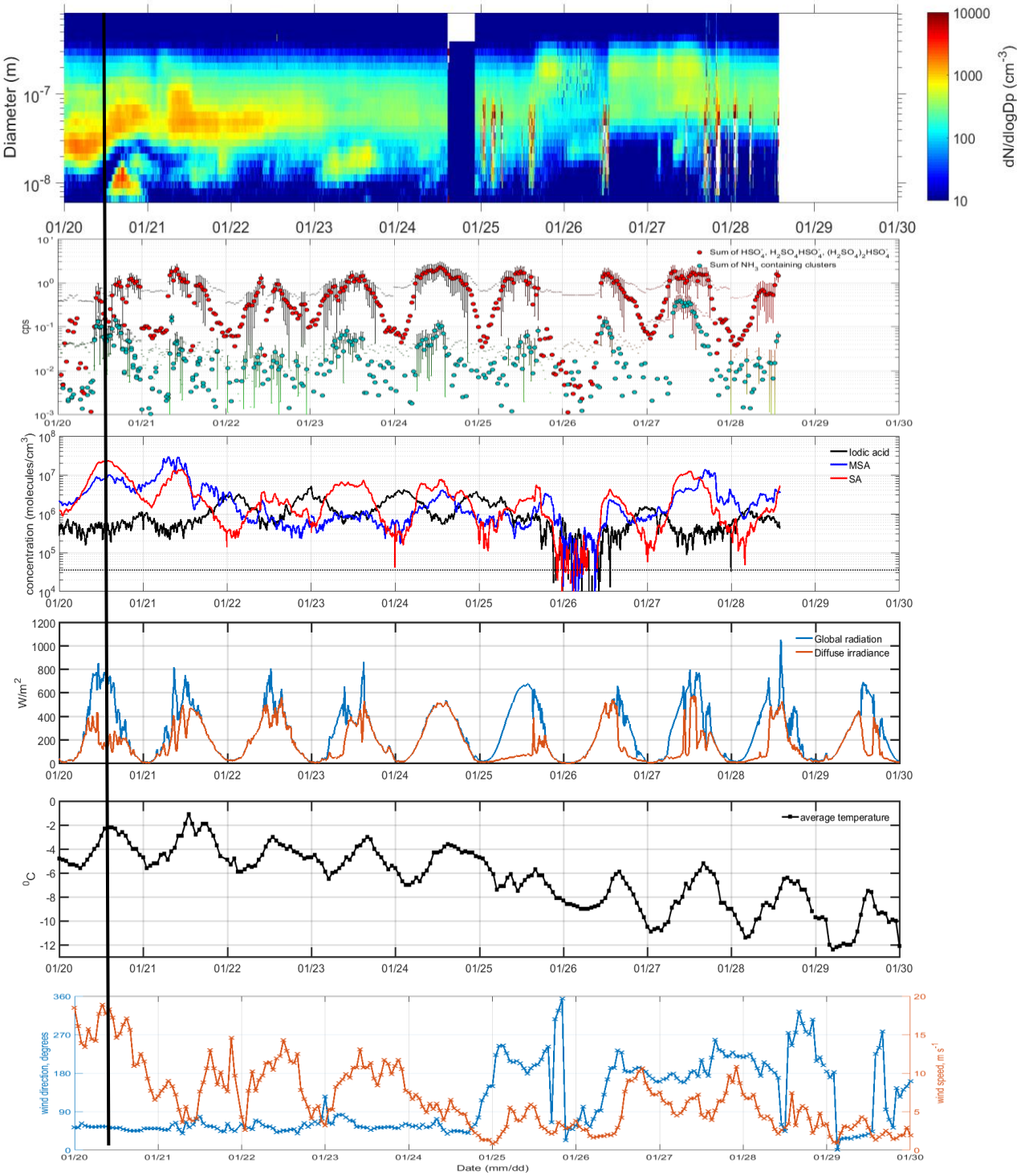
Diameter (m)
dN/dlogDp (cm-3)
10000
1000
100
10
01/20
01/21
01/22
01/23
01/24
01/25
01/26
01/27
01/28
01/29
01/30
cps
Sum of HSO4-, H2SO4HSO4-, (H2SO4)2HSO4-
Sum of NH3 containing clusters
concentration (molecules/cm3)
Iodic acid
MSA
SA
W/m2
Global radiation
Diffuse irradiance
0C
average temperature
wind direction, degrees
wind speed, m s-1
Date (mm/dd)

Fig. S1. Overview of the FINNARP-2014 campaign at Aboa, Antarctica (no flagged data). NPF events are marked with black vertical lines over the event days (3, 7-11, 13, 18, 20 Jan), selected non-event days are marked with blue vertical lines and they are representing similar meteorological conditions as the NPF days had (23 Dec 2014, 2, 4-6 and12 Jan 2015).

Subplots: (A) 1-10 December 2014, **(B)** 11-20 December 2014, **(C)** 21-30 December 2014, **(D)** 31 December 2014 -9 January 2015, **(E)** 10-19 January and **(F)** 20-29 January 2015.

Panels from **top to bottom** in each subplot:

(1) DMPS particle size distribution of 6 - 820 nm particles, units: m. Color bar: normalized number concentration, $dN/dlogD_p$

(2) APi-TOF, negative naturally charged ions, sums of sulfuric acid clusters in red (n SA = 1-3) and tetramer to higher clusters with ammonia in blue (n SA >3, n NH_3 = 0-10), The mass spectra are all integrated for 30 min: ions/s.

(3) CI-APi-TOF (NO_3^-), neutral sulfuric acid (H_2SO_4), methane sulfonic acid (CH_3SO_3H) and iodic acid (HIO_3) concentrations, units: molecules/cm^3. Limit of detection (LOD) is marked with a dashed black line at $3.6 \cdot 10^4$ molecules/cm^3.

(4) Global and diffuse irradiance measured from 1.5 m height. The measurement site is located on snow-covered surface of the glacier about 2.5 km South-East of the Aboa station, units: W/m^2

(5) Average ambient temperature. Measurements were conducted at the weather station located right next to the aerosol measurements laboratory. Units: ^0C

(6) Wind direction, units: degrees (in blue) and average wind speed, units: m/s (in red). Measurements were conducted at the weather station located right next to the aerosol measurements laboratory.

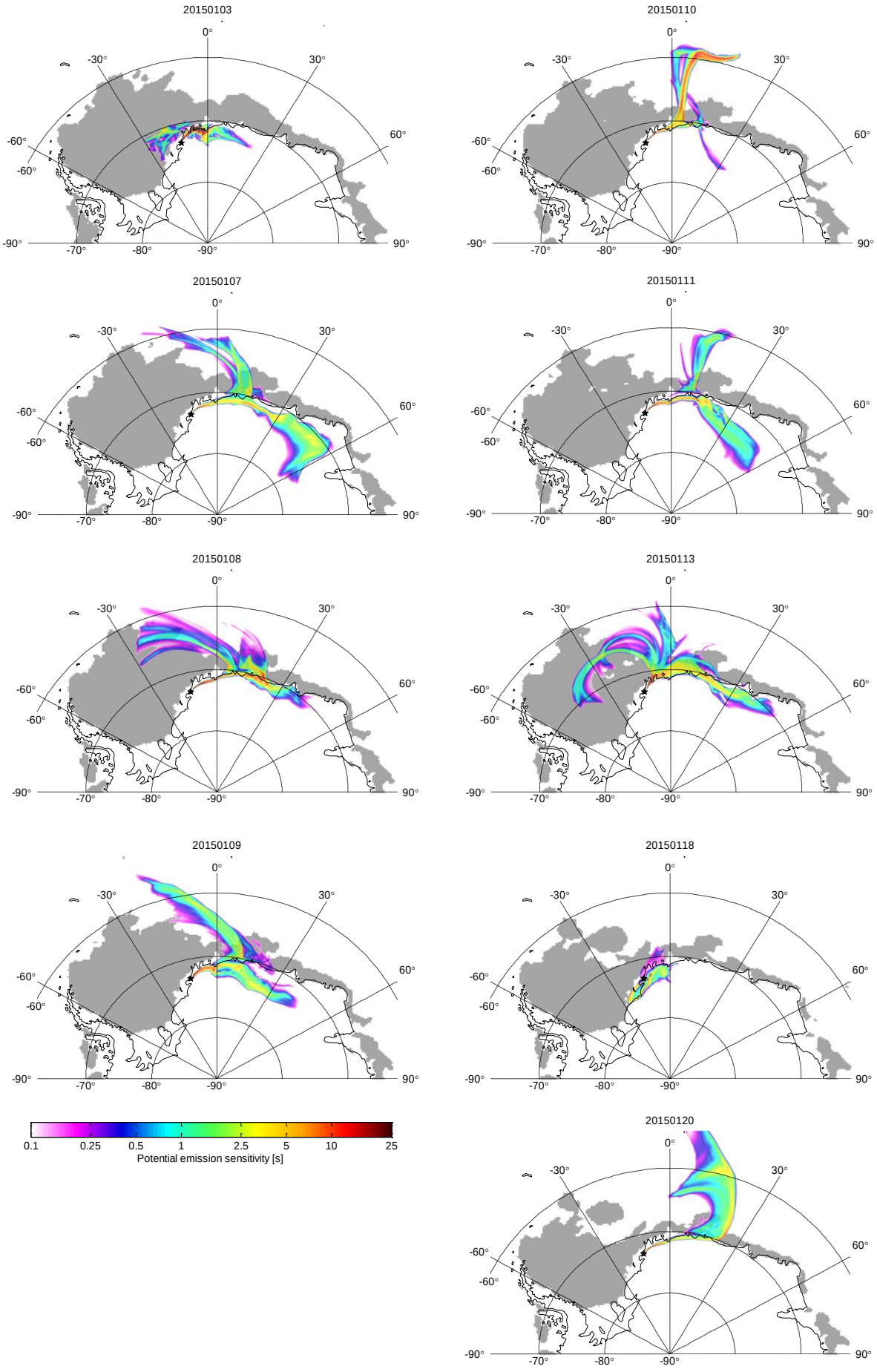
20150103
20150110
20150107
20150111
20150108
20150113
20150109
20150118
20150120
0°
-30°
30°
-60°
60°
-90°
-70°
-80°
0.1
0.25
0.5
1
2.5
5
10
25
Potential emission sensitivity [s]

Fig. S2. NPF days. Cumulative emission sensitivity of the air masses arriving to Aboa (72 h) during new particle formation days. The data present air masses in the estimated boundary layer, < 600 m in height. Sea ice (in grey, depicting areas with >25 % ice cover) covers large parts of the Weddel Sea and all NPF event air masses originated from open water condition over the Southern Ocean.

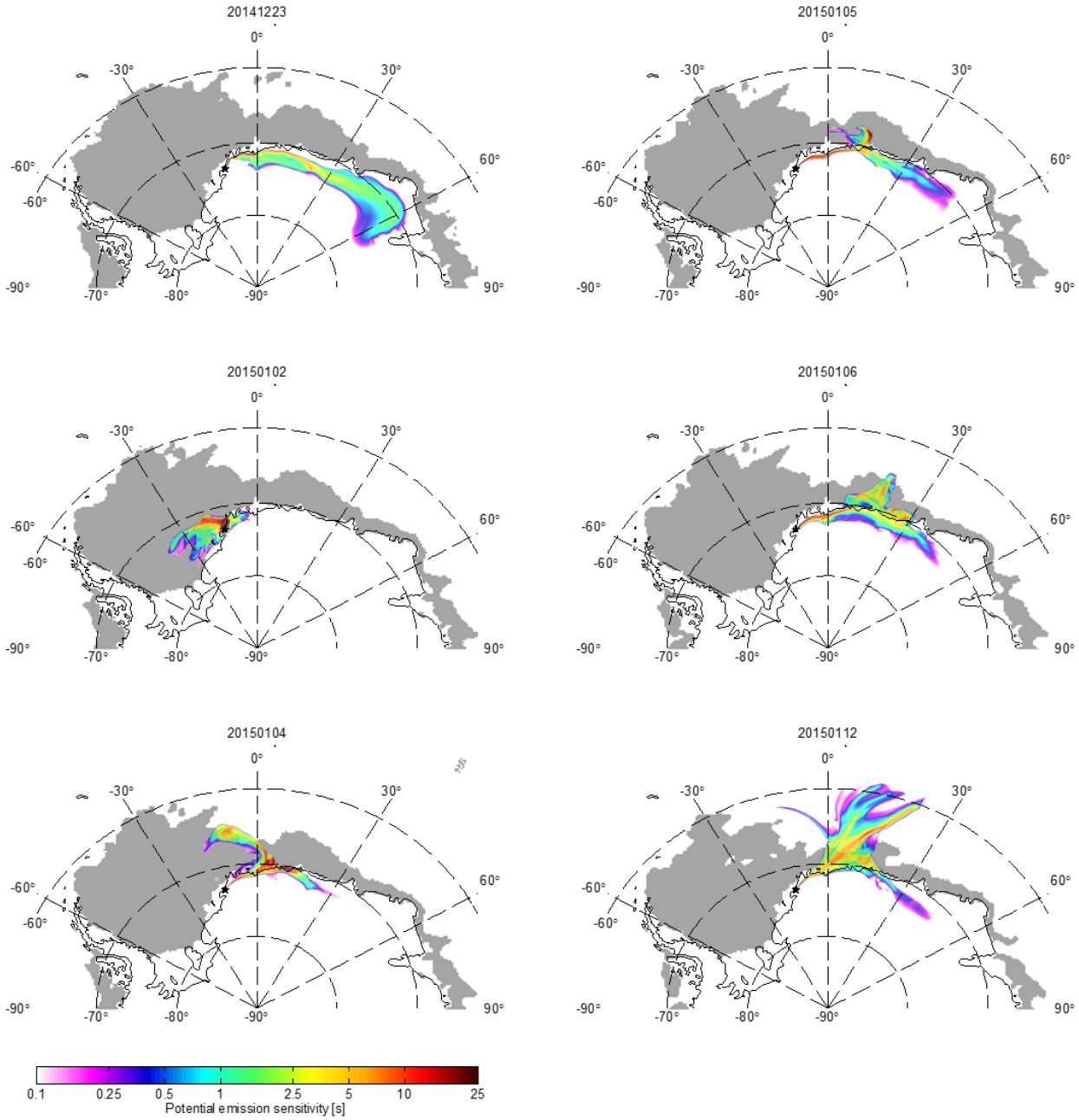

Fig. S3. No NPF days. Cumulative emission sensitivity of the air masses arriving to Aboa (72 h) during days when we did not observe new particles forming. The data present air masses < 600 m in height and these days have the same prevailing wind direction as the NPD days observed. No particle formation was observed from continental or sea ice (in grey, depicting areas with >25 % ice cover) air masses arriving to Aboa. During 12 January we only observed ion clusters of sulfuric acid, no ammonia was detected to stabilize larger cluster formation even though the air masses arrived across the open ocean.

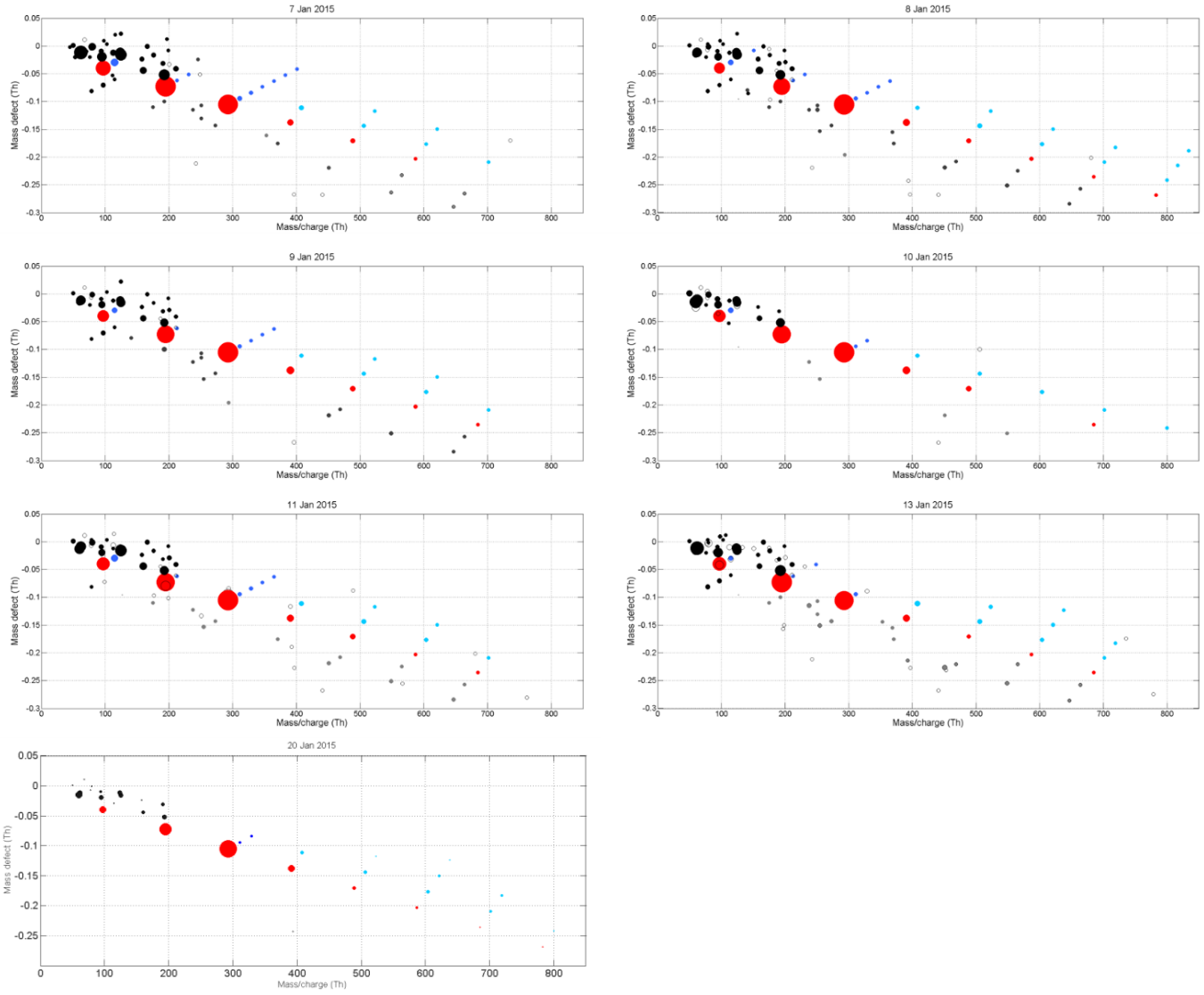

Fig. S4. Negative ion composition measured by the APi-TOF.

Negative ion mass defect plots during the observed NPF events at Aboa. Red = pure sulfuric acid clusters, light blue = sulfuric acid and ammonia clusters, blue = sulfuric acid and water clusters, grey = iodine containing compounds, black = identified compound, unfilled = unidentified compound. Mass spectra are integrated for 180 min. Top row: 7 and 8 Jan 2015, second row: 9 and 10 Jan 2015, third row: 11 and 13 Jan 2015, bottom row: 20 Jan 2015. NPF event on the 18 Jan was recorded using positive ion mode and it is depicted in Fig. S5.

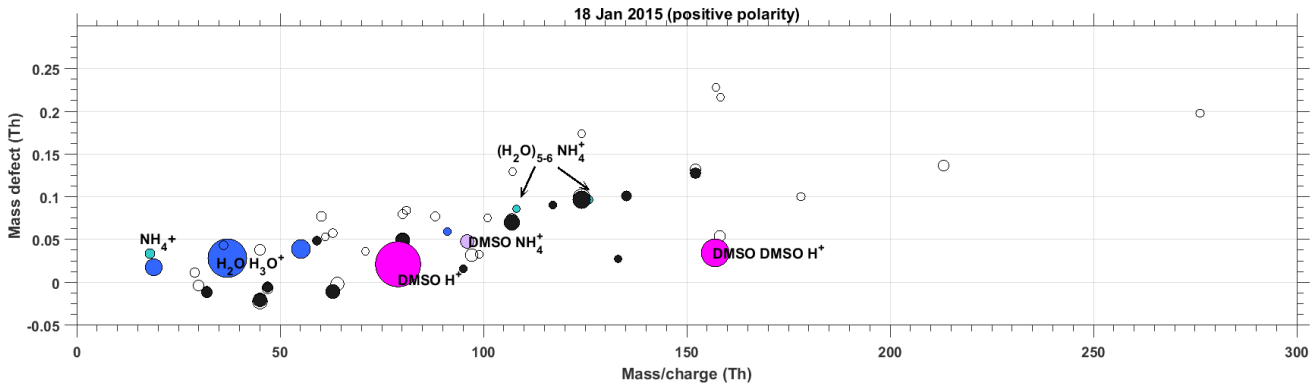

Fig. S5. APi-TOF (positive ions) mass defect plot during the observed NPF event on 18 January at Aboa. Neutral sulfuric acid concentration during the day was extremely high, up to $4(\pm2)\cdot10^7$ molecules/cm^3, yet no positive sulfuric acid-ammonia clusters were detected during this event. Data is averaged over 30 minutes. Most abundant peaks detected are dimethyl sulfoxide (DMSO, in pink), organic sulphur compound produced in dimethyl sulphide oxidation. Molecular ammonia (cyan) was detected in minute quantities and its clusters with DMSO and water were also observed during this event.

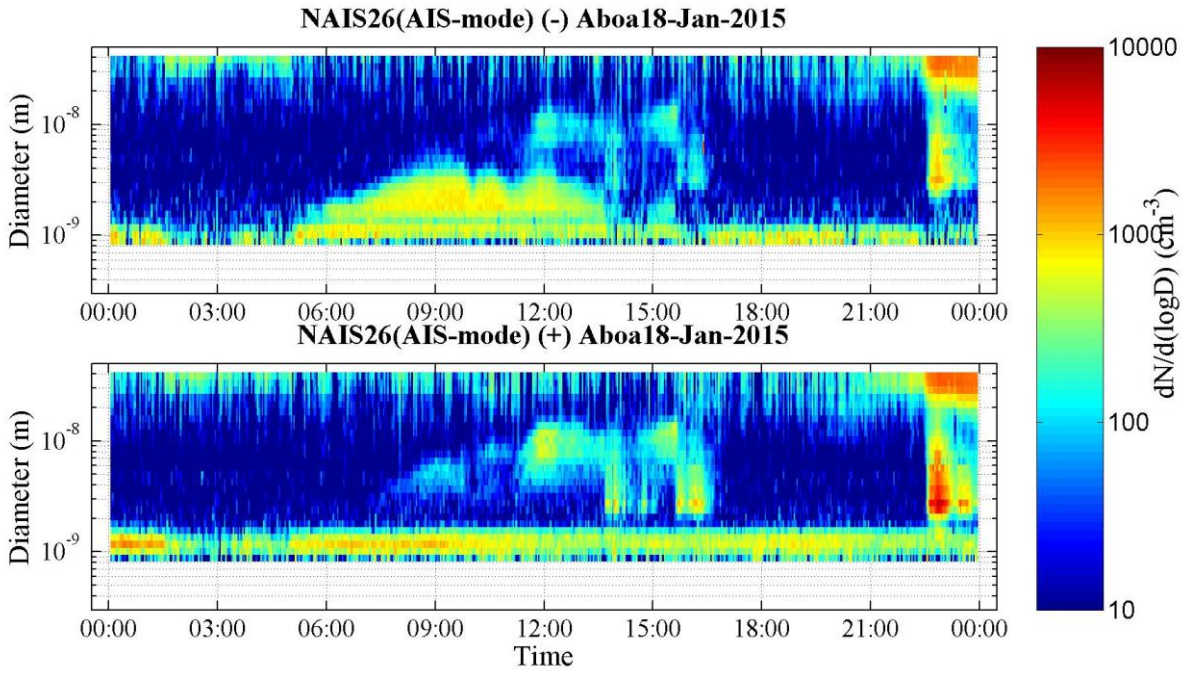

Fig. S6. NAIS size distribution of negative (top panel) and positive (bottom) ions during the NPF event day when chemical composition of ion was measured in the positive polarity (fig. S5).

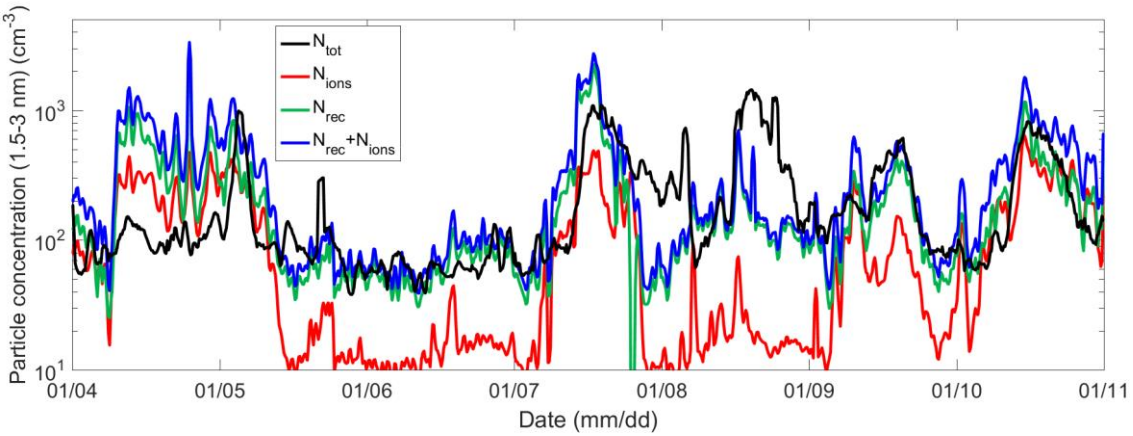

Fig. S7. Number concentrations of 1.5- to 3-nm particles during 1 week of the measurement period (4 to 10 January 2015). N_{tot} represents the concentration of 1.5–3 nm clusters measured by the Particle Size Magnifier (PSM) and N_{ions} and N_{rec} are concentrations of ions and calculated recombination products from NAIS.

A

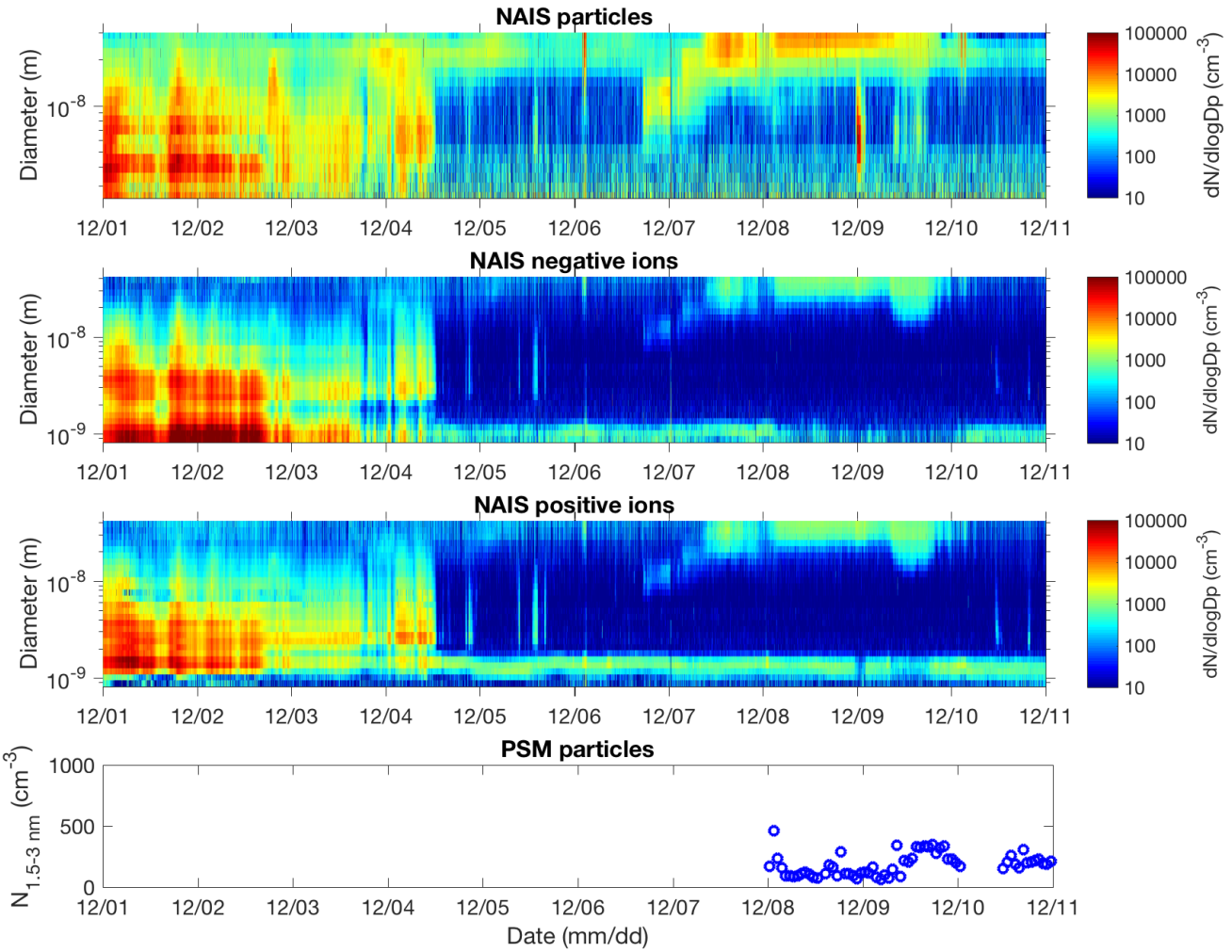
NAIS particles
NAIS negative ions
NAIS positive ions
PSM particles
Diameter (m)
dN/dlogDp (cm-3)
N1.5-3 nm (cm-3)
Date (mm/dd)
12/01
12/02
12/03
12/04
12/05
12/06
12/07
12/08
12/09
12/10
12/11

B

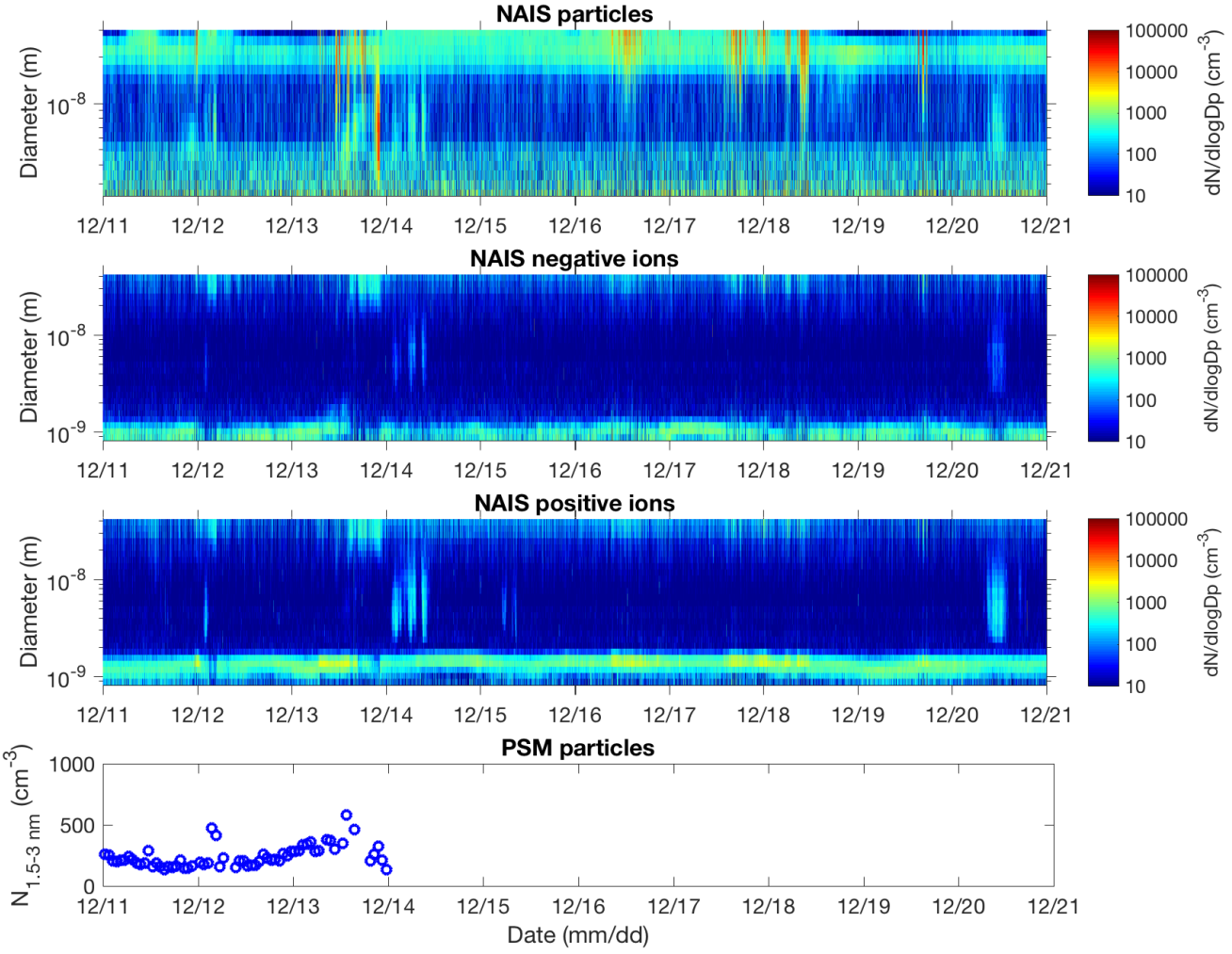
NAIS particles
NAIS negative ions
NAIS positive ions
PSM particles
Diameter (m)
dN/dlogDp (cm-3)
N1.5-3 nm (cm-3)
Date (mm/dd)
12/11
12/12
12/13
12/14
12/15
12/16
12/17
12/18
12/19
12/20
12/21

C

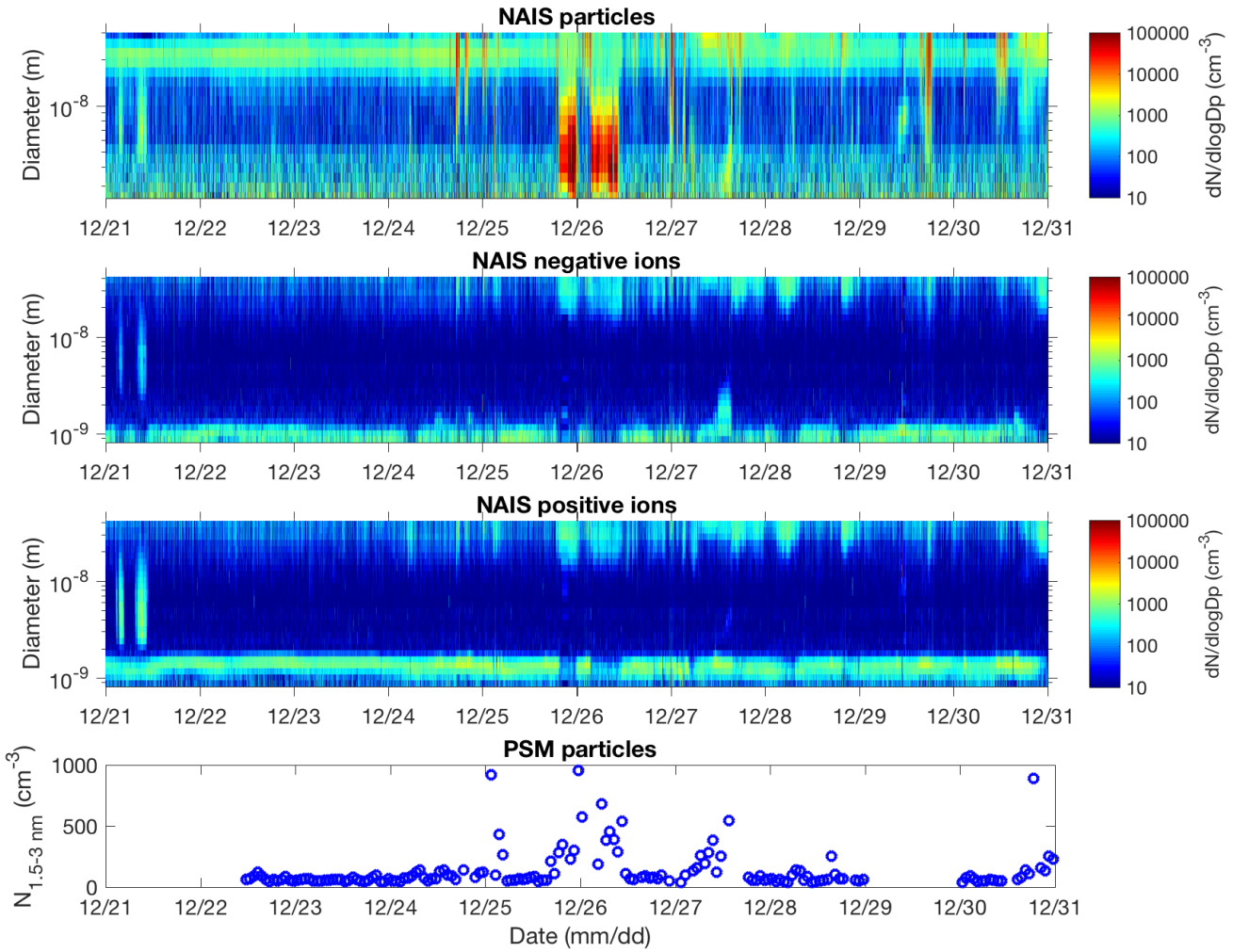
NAIS particles
Diameter (m)
10^-8
12/21
12/22
12/23
12/24
12/25
12/26
12/27
12/28
12/29
12/30
12/31
100000
10000
1000
100
10
dN/dlogDp (cm^-3)
NAIS negative ions
Diameter (m)
10^-8
10^-9
NAIS positive ions
Diameter (m)
10^-8
10^-9
PSM particles
N1.5-3 nm (cm^-3)
1000
500
0
Date (mm/dd)

D

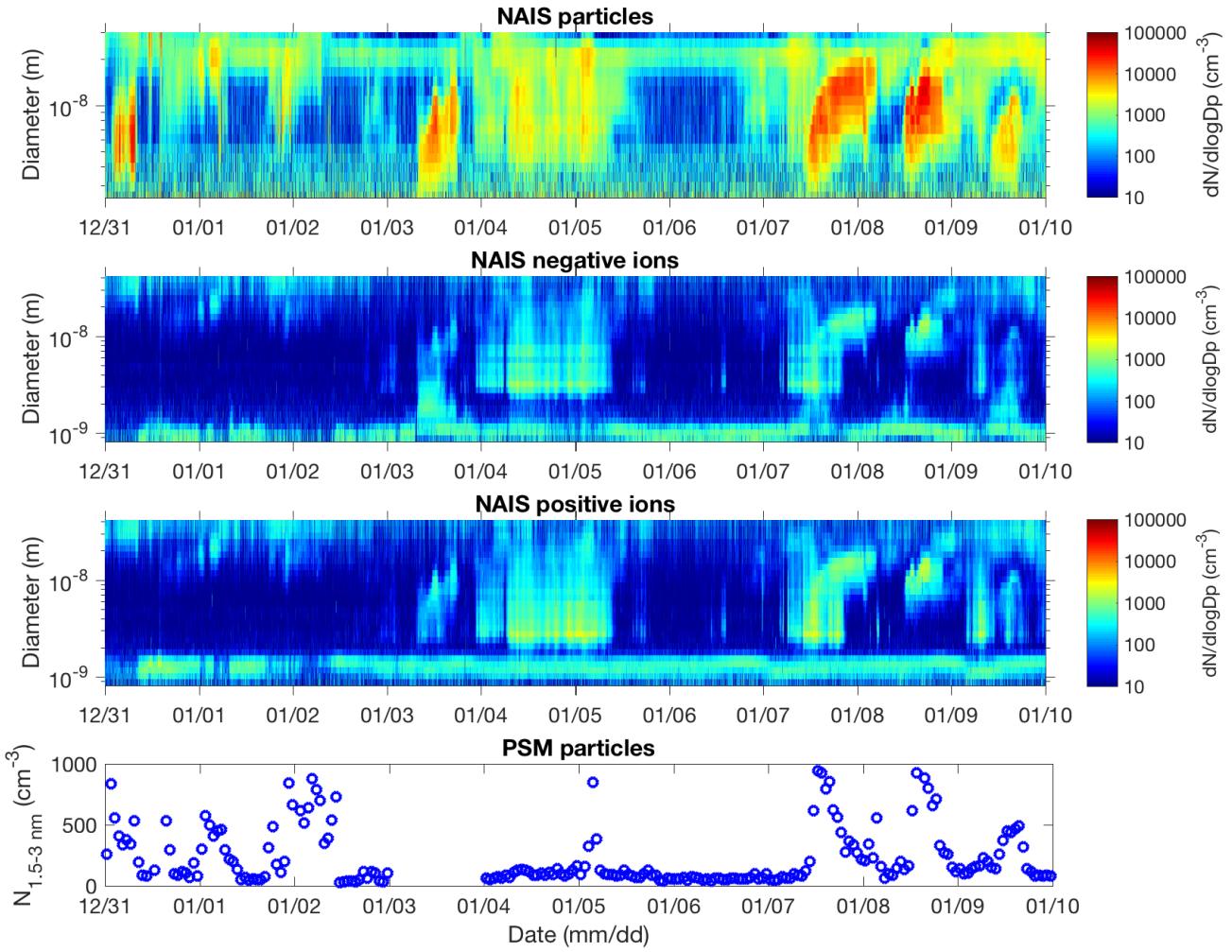
NAIS particles
NAIS negative ions
NAIS positive ions
PSM particles
Diameter (m)
dN/dlogDp (cm-3)
N1.5-3 nm (cm-3)
Date (mm/dd)
12/31
01/01
01/02
01/03
01/04
01/05
01/06
01/07
01/08
01/09
01/10

E

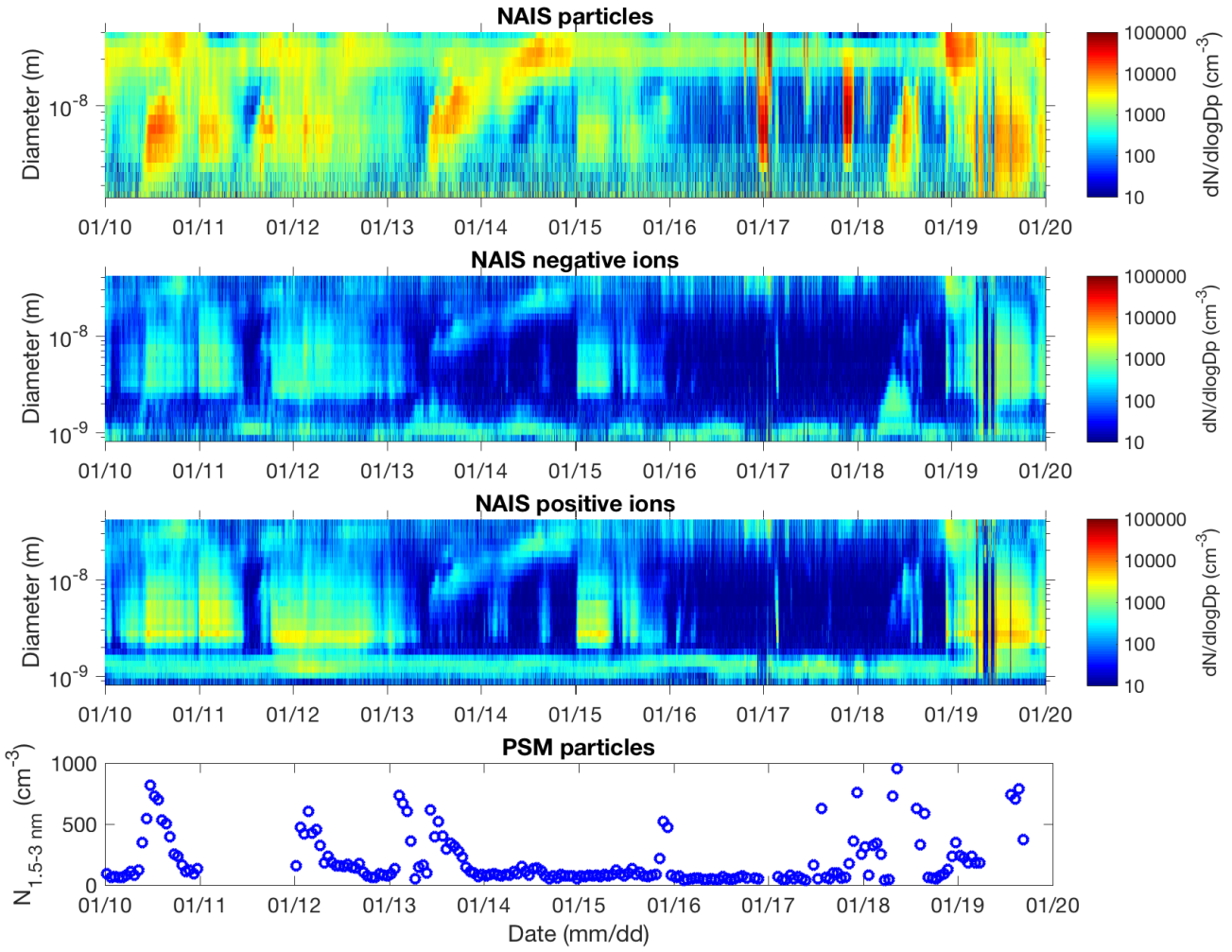
NAIS particles
Diameter (m)
10^{-8}
01/10 01/11 01/12 01/13 01/14 01/15 01/16 01/17 01/18 01/19 01/20
100000
10000
1000
100
10
dN/dlogDp (cm^{-3})
NAIS negative ions
Diameter (m)
10^{-8}
10^{-9}
01/10 01/11 01/12 01/13 01/14 01/15 01/16 01/17 01/18 01/19 01/20
100000
10000
1000
100
10
dN/dlogDp (cm^{-3})
NAIS positive ions
Diameter (m)
10^{-8}
10^{-9}
01/10 01/11 01/12 01/13 01/14 01/15 01/16 01/17 01/18 01/19 01/20
100000
10000
1000
100
10
dN/dlogDp (cm^{-3})
PSM particles
$N_{1.5\text{-}3\ nm}$ (cm^{-3})
1000
500
0
01/10 01/11 01/12 01/13 01/14 01/15 01/16 01/17 01/18 01/19 01/20
Date (mm/dd)

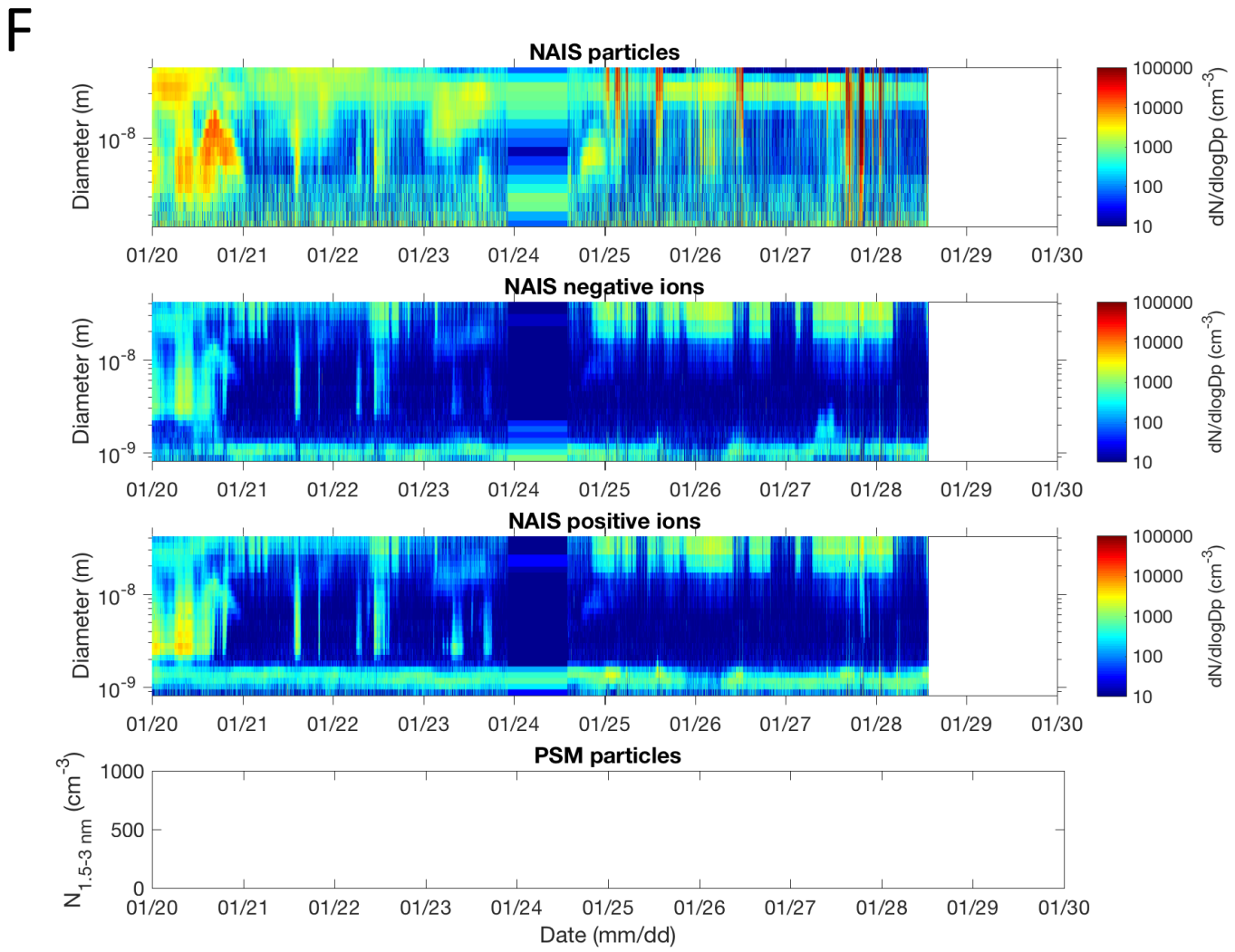

Fig. S8. The size distribution of 2- to 42-nm particles (top), 0.8- to 42-nm negative (second) and positive (third) ions measured with the NAIS, and the sum of particle concentration measured with the PSM [1.5 to 3 (±0.2) nm; bottom] during the measurement campaign. (A) 1-10 December 2014, (B) 11-20 December 2014, (C) 21-30 December 2014, (D) 31 December 2014 -9 January 2015, (E) 10-19 January and (F) 20-29 January 2015.